Title
Effect of furnace atmosphere on E-glass foaming

Journal
Journal of Non-Crystalline Solids, 352

Authors
Kim, D. S.
Dutton, Bryan C.
Hrma, Pavel R.
et al.

Publication Date
2006

Peer reviewed

Effect of furnace atmosphere on E-glass foaming

Dong-Sang Kim [a,*], Bryan C. Dutton [b], Pavel R. Hrma [a], Laurent Pilon [b]

[a] *Pacific Northwest National Laboratory, Richland, WA 99352, USA*

[b] *Mechanical and Aerospace Engineering, University of California, Los Angeles, CA 90095, USA*

Abstract

The effect of furnace atmosphere on E-glass foaming has been studied with the specific goal of understanding the impact of increased water content on foaming in oxy-fired furnaces. E-glass foams were generated in a fused-quartz crucible located in a quartz window furnace equipped with video recording. The present study showed that humidity in the furnace atmosphere destabilizes foam, while other gases have little effect on foam stability. These findings do not contradict the generally accepted "dilution model", suggesting that foaming is more severe in oxy-fired furnaces than in air-fired furnaces because the higher concentration of water in the furnace atmosphere ultimately enhances sulfate decomposition resulting in stronger foaming. The failure to reproduce this effect in

[*] Corresponding author. Tel.: +1-509 373 0256; Fax: +1-509 376 3108.
E-mail address: dong-sang.kim@pnl.gov (D. Kim)

laboratory experiments may be attributed to water incorporation into the glass melt occurring during ablation melting in industrial furnaces.

PACS code: 81.05.K

1. Introduction

Glass foams generated in glass-melting furnaces reduce energy efficiency and can lead to poor glass quality [1-8]. Foaming of E-glass refined with sulfate is especially severe when processed with oxy-fuel firing [6]. The objective of this study is to assess the effects of the furnace atmosphere, mainly its water content, on E-glass foaming. The ultimate goal is to identify conditions for foam reduction during E-glass processing.

Most of the studies on foaming in silicate melts focused on soda-silicate or soda-lime-silicate melts [2-5,9], or on metallurgical slags [10-14]. Pilon *et al.* [15] provides thorough reviews of the literature; they also collected data on foaming and correlated the extent of foaming of different high-viscosity liquids with their properties. Unfortunately, little data exist on foaming in E-glass.

Cable *et al*. [9], who studied the foaming of binary silicate melts, observed that foaming temperature was lower and foam volume was higher in wet atmospheres; also, foam was more stable in pure oxygen, whereas glass did not foam in a pure nitrogen atmosphere. Kappel *et al*. [2] observed that increasing the partial pressure of SO_2 destabilized foam. It has also been observed that foaming increases with the pull rate, the

use of recycled and contaminated cullet of mixed colors [6]. The type of gaseous fuel used to heat the melt and also the luminosity of the flame it produces were reported to affect the foam of iron slags [10].

It is generally believed that severe foaming in oxy-fuel-fired furnaces is caused by a higher partial pressure of water in the furnace atmosphere [6]. However, even for soda-lime glasses and metallurgical slag, the effect of water on foaming is not clearly understood and reported experimental data appear to be contradictory. For example, Cable et al. [9] and Laimböck [6] reported that wet atmosphere increased foaming, whereas Kappel et al. [2] showed that humidity in the atmosphere destabilized the foam. Water reduces viscosity, thus reducing foam stability by enhancing foam drainage. Water also reduces surface tension [16]. According to Parikh [16], polar gases such as sulfur dioxide (SO_2), ammonia (NH_3), hydrogen chloride (HCl), and water vapor (H_2O) lower the surface tension, whereas nonpolar gases such as dry air, dry nitrogen, helium and hydrogen have no effect. Among the polar gases cited, water has the largest dipole moment and therefore has the strongest effect on the surface tension. Parikh [16] showed that the surface tension decreases with the square root of the partial pressure of water. However, the effect of surface tension on foam stability depends more on its change with time or its gradient across the foam film thickness separating the bubbles.

Laimböck [6] studied the effect of water content on the foaming of soda-lime glass batch in air atmospheres and found that the foam formation started at a lower temperature and the maximum foam volume (and total foam volume) increased as the water content in air increased from 0 to 55%. Laimböck [6] measured the sulfate content in glass before and

after foaming and found that the sulfate loss during foaming increased as the water content increased. This increased sulfate loss (lower sulfate retention) at higher water content was responsible for higher foaming. As dissolved water content in glass increases, the partial pressure of H_2O in bubbles also increases, thus diluting the fining gas concentration in bubbles and promoting the transfer of fining gases from the melt into bubbles. In other words, water vapor in bubbles decreases the partial pressure of fining gases, thus increasing the driving force for their transfer from melt and shifting the equilibrium reaction towards a more extensive decomposition of the fining agents. As a result, sulfate begins to decompose at a lower temperature resulting in lower sulfate retention. This mechanism was formulated as the "dilution model" [6]. Water in the furnace atmosphere helps the refining action of the sulfate, making it possible to lower the addition of sulfate to obtain an equal refining efficiency compared to dry atmosphere.

Numerous laboratory studies used one of the following two methods for foam generation in molten glass: (i) refining gases are generated by increasing temperature or reducing pressure; this creates transient foam that grows and collapses [2-6,9] (ii) gas is bubbled through a glass melt at a constant temperature; this produces a steady state foam of constant height [2,6]. This study evaluates the stability of transient foams generated from E-glass by increasing temperature under various atmosphere compositions, including CO_2, O_2, N_2 and H_2O.

2. Experiments

A box furnace with a fused-quartz window at the front door was used in foaming experiments. A sample of glass batch in the form of loose blanket was placed in a fused-quartz cylindrical crucible of 2 cm inner diameter and either 10 or 30 cm in height. The glass batch used in this study was an industrial E-glass batch mix of fine-sized raw materials (typically <40 μm in diameter). The as-poured loose batch was used without an effort to make the packing density of the batch constant by tapping or similar action. The sample height-to-width ratio was recorded by a video camera and the sample height was determined from the known inside diameter of the cylindrical crucible. The furnace had a rear recess that was kept at a lower temperature than the crucible area to provide a darker background for a better contrast at high temperatures. The glass batch used in this study was an industrial E-glass batch mix containing 0.14 wt% Na_2SO_4, which leads to a target concentration of 0.17 wt% SO_3 in glass including the sulfate introduced as impurity from other raw materials.

Two initial foam experiments were conducted under ambient atmosphere using a 10 cm high crucible by ramp heating the batch from 300 to 1500°C and holding it at 1500°C for 30 min: one with a 5 g batch and a heating rate of 10°C/min and the other with 4 g batch and heating rate of 5°C/min.

The foam experiments under controlled gas atmosphere were performed with a 4 g batch contained in a 30 cm high crucible heated at 5°C/min from 300°C to 1500°C. These conditions produced an adequate maximum foam height for our experimental setup; 5°C/min is believed to simulate the typical heating rate of the batch in actual glass furnaces [17].

Fig. 1 shows a schematic of the experimental setup used for the study of E-glass foaming under controlled atmospheres. The batch was initially heated under ambient atmosphere and the gases, such as air or carbon dioxide, were introduced into the crucible once the temperature reached 1250°C. Humidity was controlled by bubbling compressed gas through water in a flask that was kept at a constant temperature. The path of the gas from the flask to the crucible was heated via insulated resistive heating coil wrapped around the gas tube to prevent condensation of water in the gas inlet system. The tip of the gas inlet tube was positioned well above the melt surface to minimize its effect on the temperature inside the crucible. For the same reason, the heating coil was turned on in all tests regardless of humidity in the gas mixture.

The gas flow rate was set to 40 cm^3/min for most tests. This flow rate was deemed sufficiently low to avoid mechanical agitation of the foam and a decrease of the temperature above the melt while maintaining a constant atmosphere. At this flow rate, the gas content in the crucible would be renewed roughly every 2 min. The flow rate of gas was measured before the gases were humidified; thus, the actual flow rate was higher for atmospheres containing H_2O. Table 1 summarizes the test conditions used in the present study. It is assumed that dry air was composed of 80% N_2 and 20% O_2 and the gases introduced into the flask reached equilibrium H_2O concentration. Although the amount of H_2O in each condition was not measured, it is assumed that the actual water content does not significantly deviate from the calculated value given the slow gas flow rate.

3. Results

Fig. 2 and Fig. 3 show the sample height and furnace temperature changes over time for two initial foam experiments performed under ambient atmosphere: one with a 5-g batch and a heating rate of 10°C/min and the other with 4-g batch and a heating rate of 5°C/min. The batches sintered and started to melt at temperatures between 1120 and 1140°C. Then, the melt height began to increase due to foaming at about 1370°C for both experiments. The maximum foam height was reached within the observable range for the test with 4-g batch and 5°C/min heating rate (Fig. 3). For the test with 5-g batch and 10°C/min-heating rate (Fig. 2), the foam eventually rose beyond the observable range of the present set-up. The collapse side of the foam-height curve (marked by the dotted line) was subjected to uncertainty because the visibility of the foam height was decreased by the glass melt attached to the crucible wall. Fig. 4 compares the height of the samples per unit mass of batch, i.e., h/m_B, where h is the foam height and m_B is the mass of the batch. Assuming that the gas phase is uniformly distributed throughout the glass phase, the foam volume per batch mass is $v_{FB} = Ah/m_B$, where A is the cross-sectional area of the cylindrical crucible.

Fig. 4 shows that the maximum foam height is lower when the heating rate is slower. This observation can be rationalized as follows. Let us suppose for simplicity that the gas phase produced from decomposing sulfate remains entrapped in the melt until the melt reaches a certain high temperature T_2; say T_2 = 1470°C, at which the gas phase is rapidly released. Let us further assume that the sulfate begins to decompose at a certain temperature T_1; say T_1 = 1370°C (both temperatures were arbitrarily chosen for the sake of

illustration). Let v_G be the volume of gas generated in the melt and R_a the average rate of gas release from the foam within the temperature interval from 1370°C to 1470°C and $\Phi = dT/dt$ the rate of temperature increase (where T is the temperature and t is time). Then the volume of gas retained in the foam when temperature is raised from 1370°C to 1470°C is $v_F = v_G - R_a(t_2 - t_1)$, where t_1 and t_2 are the times at which the sample temperature was T_1 and T_2 , respectively. If the heating rate is constant, then $v_F = v_G - R_a(T_2 - T_1)/\Phi$. It follows that the volume of gas retained within the melt increases as the heating rate increases.

As shown in Fig. 4, the initial batch height per unit mass of batch, which is proportional to the batch specific volume, varies considerably from one experiment to another. This is caused by differences in packing density of batch particles in each experiment, which was not a variable deliberately controlled. However, as expected, the melt height beyond 1200°C and before foaming is similar in both experiments; the volume varies according to the content of gas phase in the samples. The final height per unit mass of batch of the refined melt after the collapse of the foam was the same for all experiments.

The results from foaming experiments under controlled atmosphere are shown in the form of gas phase-to-liquid phase volume ratio, ψ, defined as $\psi = V_g/V_m$ where V_g is the volume of gas in the sample and V_m is the volume of melt in the sample. Obviously, $V_g = V - V_m$, where V is the total volume of foam. Hence, since the sample is contained in a vertical cylindrical column of constant cross-sectional area,

$$\psi = \frac{H}{H_m} - 1 \qquad (1)$$

where H is the sample height and H_m is the height of a gas phase-free sample. The value of H was measured from the video recording while H_m was calculated using the formula

$$H_m = \frac{m_b f_b}{A \rho_m} \tag{2}$$

where m_b is the mass of the batch loaded into the crucible, f_b is the melt-to-batch mass ratio, A is the crucible inner cross-sectional area, and ρ_m is the melt density. For the present E-glass, f_b = 0.899, ρ_m = 2.45 g/mL at 1350°C, $A = \pi r_c^2$, where r_c = 10 mm is the crucible inner radius, and m_b = 4.00 g for all experiments leading to H_m = 4.67 mm.

Fig. 5 displays ψ and T as functions of time for the tests with air flow. The target temperature history (ramping at 5°C/min to 1500°C) is also shown. To avoid the time shift between experiments, the time was set to zero when the furnace temperature reached 1300°C. Typically, ψ reaches a maximum at a temperature below 1500°C. As Fig. 5 shows, the actual temperature history somewhat differs from the targeted one (the rate of heating slows down before reaching the final temperature) and the final temperature slightly differs from experiment to experiment, but the time-temperature curves up to the final temperature are almost identical. The inability to keep the final temperature the same in every experiment was inherent to the experimental setup. Hence, the foam starting temperature, the maximum foam height, and the foam generation rate occurred under well-controlled experimental conditions, whereas the foam collapsed at temperatures that were not exactly identical, not to mention the poor visibility of the collapsing sample caused by bursting of bubbles that obscured the crucible wall.

For the three tests with air flow, for which ψ versus t is displayed in Fig. 5, the average maximum value, ψ_{max}, was 7.00 with a standard deviation of 0.46, corresponding to a reproducibility conservatively estimated at 13%.

Fig. 6 through Fig. 8 show the evolution of ψ versus time for experiments conducted under various atmospheres: (i) dry and humid air (Fig. 6), (ii) dry and humid CO_2 (Fig. 7), and (iii) various dry atmospheres (Fig. 8). Fig. 6 and Fig. 8 include ψ versus t for the Test #1 (air) from the three tests with air flow. Table 2 summarizes the values of ψ_{max}, used as a key measure of foaming extent, for all tests.

The melt expansion rate, defined as $r_\psi = \mathrm{d}\psi/\mathrm{d}t$, is another indicator of foam behavior. As illustrated in Fig. 2, two intervals on which r_ψ is nearly constant can be distinguish on the foaming curve. The first is the "primary" interval, where pre-existing bubbles expand with increasing temperature. The second is the "fining" interval, where the bubbles grow as a result of fining reactions. The corresponding two r_ψ values were obtained from data points on these nearly linear portions of the foaming curve. The low-temperature r_ψ values are virtually identical for all tests. Table 2 also summarizes r_ψ and $\mathrm{d}\psi/\mathrm{d}T$ values (obtained from the plots of ψ versus temperature) for the fining interval, time range for r_ψ, and foam starting temperature. The foam starting temperature was determined as the temperature at which the fining interval begins (see Fig. 2).

The foam decay is the least reproducible process under the present test conditions. It is governed by the rate of bursting of bubbles, which is a random process. In addition, as mentioned above, the temperature at the maximum foam height slightly varied from experiment to experiment. Nevertheless, the duration of foam collapse was measured and the results are summarized in Table 2. The symbols $t_{0.5}$ and $t_{0.25}$ represent the times for the foam to collapse to $0.5\,\psi_{\max}$ and $0.25\,\psi_{\max}$, respectively. Note that some samples did not reach $0.25\,\psi_{\max}$ before the test was terminated. The estimated errors for ψ_{max}, $\mathrm{d}\psi/\mathrm{d}t$ (or

$d\psi/dT$), $t_{0.5}$, and $t_{0.25}$ summarized in Table 2 are ±7%, ±22%, ±24%, and ±24%, respectively, based on relative standard deviation from triplicate tests under air atmosphere (Tests #1 through #3). For $t_{0.25}$ the same percent relative standard deviation as for $t_{0.5}$ was assumed.

Fig. 9 and Fig. 10 show the ψ_{max} and $d\psi/dT = (d\psi/dt)/(dT/dt)$, as a function of H_2O vol%; Fig. 11 and Fig. 12 show $t_{0.5}$ and $t_{0.25}$ as a function of H_2O vol%. Error bars representing estimated errors discussed above are included in Fig. 9 through Fig. 12.

Based on these plots, the major observations can be summarized as follows:

1. The foaming extent decreased as the gas humidity increased, except for 0 to 20 vol% H_2O in air. Changing air for CO_2 while keeping the same fraction of water vapor had little effect on foaming when humidity was 20 to 55 vol% H_2O.
2. The foaming extent was lower in dry air than in other gases tested (pure CO_2, CO_2 + 20% O_2, CO_2 + 20% N_2, and CO_2 + 80% N_2). There was no other noticeable effect of dry gas composition on foaming.
3. The 10% O_2 addition to CO_2 with 55% H_2O had no noticeable effect on foaming.
4. No noticeable trend was observed in foam starting temperature between tests (1365 to 1385°C) except in air with 55% H_2O, where the foam starting temperature was noticeably higher (1404°C). Note that Laimbock [6] found a decrease in foaming temperature of soda-lime silicate glass caused by the presence of water vapor.

4. Discussion

4.1 Foam stability

Foam stability can be measured using ψ_{max}, $d\psi/dT$, or $t_{0.5}$. Experimental results show that the stability of E-glass foam decreased with increasing humidity level (Fig. 9 through Fig. 12). This was most likely caused by the decrease in viscosity of the melt films in the top foam cells caused by an increase of water content in the films (see [18] and [19] for the effect of water on the viscosity of glass melts).

Except for dry air and water vapor, the atmosphere composition had no noticeable effect on foam stability. This is particularly true for the excess O_2 in simulated oxy-fired environment. These observations indicate that changing the furnace atmosphere, if such a change was technologically and economically feasible, is not expected to reduce the current level of foaming.

The foam-destabilizing effect of dry air as compared to other dry gases is not understood at present. Additional experiments that would verify and elucidate this observation were not performed in the present study as they appear irrelevant to the objective of the current research, which is to identify conditions for reducing foaming in oxy-fired furnaces.

4.2 Effect of water on refining reactions and foaming

According to Laimböck [6] and Beerkens *et al.* [20], increased foaming that occurs in oxy-fired furnaces is caused by increased humidity of the furnace atmosphere, referred to

as “dilution model”. As described in Section 1, increased humidity of the furnace atmosphere increases the water content in the glass melt and the water partial pressure in gas bubbles. Water dilutes fining gases that have diffused in the bubbles from the melt. The decrease in concentrations promotes the transfer of fining gases from the melt into the bubbles. This dilution model is well developed mathematically and is supported by strong experimental evidence from foaming studies conducted on soda-lime glasses [6, 20]. The extent of foam will be determined by the relative magnitude of two opposing effects of dissolved water which depends on glass type and melting conditions. It destabilizes the foam by reducing the glass melt viscosity, on the one hand, and enhances foaming due to gas dilution effect in the bubble, on the other.

In our experiments with E-glass except Test 13, the possibility of significant water dissolution in glass at early stages of melting, and thus the dilution effect, was minimized by introducing humid gas only after the batch reactions were completed. However, contrary to the expectation, Test 13 in which the humid gas (45% CO_2 + 55% H_2O) was introduced at early stages of melting did not produce any foam, whereas Test 8 with same humid atmosphere introduced at 1250°C produced foam. The lack of foaming in Test 13 was most likely caused by a loss of sulfate at $T < 1250$°C due to higher water content at early stages of melting. Sulfate loss by evaporation is promoted by humidity and proceeds at temperatures well below the sulfate decomposition temperature. If losses due to evaporation are such that the partial pressures of SO_2 and O_2 in glass are too low to cause an appreciable growth of bubbles, no foaming will occur. However, this effect is probably insignificant when melting occurs on a large scale. In E-glass melting furnace, water vapor

may penetrate into the loose batch and dissolve in the melt to produce the dilution effect discussed above without causing a substantial loss of sulfate. Hence, the dilution effect cannot be ruled out based on a crucible melt experiment.

Dilution effect is considered the main cause of increased foam in melting soda-lime glass in oxy-fired furnaces. Therefore, it is worthwhile taking a closer look at the differences between fining soda-lime glass and E-glass. Laimböck [6] measured the sulfate loss in soda-lime glass at early stages of melting as well as during fining. The initial SO_3 concentration in the soda-lime glass was 0.66 wt%, the SO_3 concentration before fining decreased to 0.55~0.53 wt%, and was 0.32~0.15 wt% after fining. These numbers are large compared to the as-batched SO_3 concentration in E-glass of the present study, which was ~0.17 wt% (roughly half of this amount came from Na_2SO_4 and the rest was impurities from other raw materials, mainly colemanite). Estimating that SO_3 concentration dropped to 0.01 wt% after fining (typical measured concentration in the product glass), and considering possible evaporation of sulfate before fining, one can conclude that less than 0.16 wt% SO_3 produced foaming in E-glass. This is a very small amount compared to soda-lime glass. Consequently, a relatively small loss of sulfate from E-glass may decrease the gas generation rate below the foaming threshold that may be not too far below 0.16 wt% SO_3. (The content of carbon or any reducing agent in the batch would affect the concentration of SO_3 in the glass melt formed after the batch melting and eventually the fining and foaming. Reducing agent was not added to the batches for crucible studies discussed here).

To check the above hypothesis, selected glasses from foaming experiments were analyzed for sulfate concentration. Two additional experiments (Tests 1a and 13a) were performed to determine the SO_3 content in glasses at 1250°C: the batches were heated at 5°C/min under ambient atmosphere and 45% CO_2 + 55% H_2O atmosphere and the resulting melts were air quenched when temperature reached 1250°C. Sulfur concentration was determined by inductively coupled plasma-atomic emission spectrometry after digesting the glass with a mixture of concentrated nitric, perchloric, hydrofluoric and hydrochloric acids. The results are summarized in Table 3. Estimated uncertainty for SO_3 concentration is ±15%. Fig. 13 shows a plot of SO_3 wt% versus temperature for three sets of atmosphere conditions. Error bars represent an estimated analytical uncertainty of ±15%.

During heating from 300 to 1250°C, the batch treated under 45% CO_2 + 55% H_2O atmosphere lost ~80% of the batched sulfate whereas the batch heated under ambient atmosphere had no measurable sulfate loss within analytical uncertainty. This result confirms our reasoning that the lack of foaming in Test 13 was caused by a loss of sulfate at T < 1250°C due to a higher humidity at early stages of melting. During heating from 1250 to 1500°C, the batch heated under 45% CO_2 + 55% H_2O atmosphere had a somewhat larger sulfate loss than the batch heated under air flow. This suggests that introducing the humid gas flow from 1250°C also produced the dilution effect to some extent. However, reduced foaming under humid atmospheres observed in the present study of crucible melting conditions suggests that the effect of decreased surface viscosity by water (that decreases foam) outweighed the dilution effect (that increases foam).

Not only fining and foaming behaviors of E-glass and soda-lime glass in laboratory experiments are substantially different due to differences in their sulfate content but also large differences exist between crucible and furnace melts. The scale and geometry of melting in industrial furnaces is very different from crucible experiments, and, consequently, the batch and glass melt are subjected to a different thermal history. Thus, increased E-glass foaming in industrial furnaces during oxy-firing could be caused by the dilution effect that has not been reproduced in the present laboratory crucible experiments.

In industrial furnaces, water can enter the glass melt at several stages of the glass melting process. First, it can directly dissolve in the melt through its free surface. However, this mode of dissolution can hardly affect fining even at a high rate of surface renewal because the melt is deep and its surface-to-volume ratio is rather small. Given the average residence time of the melt in the furnace, this mechanism would hardly allow a sufficient amount of water to diffuse into the melt and affect the bubble growth deep in the fining area. Second, water can dissolve into the glass melt from the furnace atmosphere through the foam. Here also, the fining process cannot be significantly affected by the diffusion of water into the foam except in the top bubbles, where it destabilizes the foam rather than promoting it. Third, water can be introduced in glass during the ablation process as discussed below.

A realistic opportunity for water to dissolve in glass during large-scale industrial processes occurs at the stage when logs or piles of glass batch are melted through the ablation mechanism. This mechanism was discovered and described by Hammel [21] (see also Woolley [22]). The surfaces of logs or piles of glass batch melt upon heating by

thermal radiation from gas-burning flames. The early melt that contains undissolved refractory particles, such as those of silica, and gas bubbles, flows down on the logs' inclined surfaces, exposing deeper and deeper masses of the batch to thermal radiation until the entire batch pile is melted. In the case of soda-lime glass, the early melt contains a high fraction of alkalis (because silica particles are not fully dissolved) and thus has an ability to retain sulfate while water is being absorbed from the atmosphere. A similar ablation process operates in the case of the alkali-free E-glass made from fine-grained batches, though the content of undissolved silica particles in the early melt and its effect on sulfate retention are different from soda-lime glass. However, the final result with respect to water incorporation and sulfate retention appears to be similar in both E-glass and soda-lime glasses. The ablation process was not reproduced in our experimental arrangement, in which evaporation or early decomposition decreased the sulfate concentration to a level below the foaming threshold, thus causing the failure of producing foam when the humid atmosphere was introduced from the beginning of the experiment.

In a rather simplistic argument, if the only purpose of adding sulfate to E-glass batch were to control the refining behavior, as in a typical clear soda-lime glass, the dilution effect in oxy-fired conditions would require a smaller addition of sulfate to achieve the same refining efficiency and would decrease foaming. However, sulfate in E-glass serves also other purposes than refining, such as redox control. These other functions of sulfate require a minimum sulfate level that may be above the foaming threshold. Increased foaming can be dealt with in conjunction with E-glass melting and forming as a whole.

5. Conclusions

The results of foaming experiments with varying gas atmospheres conducted in this study rule out the possibility that increased foaming in oxy-fired E-glass melting furnaces (compared to air-fired) is caused by the effect of water or other gases on foam stability. It is suggested that the dilution effect of water on sulfate decomposition by increased partial pressure of water in bubbles that promote the transfer of fining gases from the melt into bubbles, discussed in the literature primarily for soda-lime glasses, is also a contributing cause of increased foaming in E-glass under oxy-fuel conditions.

Acknowledgements

This work was supported by the U.S. Department of Energy's Office of Industrial Technologies (OIT) in conjunction with The Glass Manufacturing Industry Council (GMIC). The authors would like to thank PPG Industries, Corp., Ms. Cheryl Richard and Dr. Hong Li for helpful technical discussion and for supplying the E-glass batch. Pacific Northwest National laboratory is operated by Battelle for the US Department of Energy under contract DE-AC05-76RL01830.

References

[1] W, Trier, Glastech. Ber. 48 (1975) 181.

[2] J. Kappel, R. Conradt, H. Scholze, Glastech. Ber. 60 (1987) 189.

[3] D. Kim, P. Hrma, J. Am. Ceram. Soc. 74 (1991) 551.

[4] D. Kim, P. Hrma, J. Am. Ceram. Soc. 75 (1992) 2959.

[5] P. Hrma, D. Kim, Glass Technol. 35 (1994) 128.

[6] P. Laimböck, Ph.D. Thesis, University of Technology, Eindhoven (1998).

[7] A.G. Fedorov, R. Viskanta, Phys. Chem. Glasses 41 (2000) 127.

[8] A.G. Fedorov, L. Pilon, J. Non-Cryst. Solids 311 (2002) 154.

[9] M. Cable, C. G. Rasul, J. Savage, Glass Technol. 9 (1968) 25.

[10] C.F. Cooper, J.A. Kitchener, J. Iron Steel Inst. 193 (1959) 48.

[11] Y. Zhang, R.J. Fruehan, Metall. Mater. Trans. 26B (1995) 803.

[12] S.M. Jung and R.J. Fruehan, ISIJ International, 40 (2000) 348.

[13] D. Skupien and D.R. Gaskel, Metall. Trans. B, 31B (2000) 921.

[14] M.Y. Zhu and D. Sichen, Process Metall., Steel Res. 71 (2000) 76.

[15] L. Pilon, A. G. Fedorov, and R. Viskanta, J. Colloid Interface Sci. 242 (2001) 425.

[16] N.M. Parikh, J. Am. Ceram. Soc. 41 (1958) 18.

[17] P. Hrma, Glastech. Ber. 55 (1982) 138.

[18] H. Scholze, Glass: Nature, Structure, and Properties, Springer-Verlag, 1990.

[19] K. Kitazawa, A. Kishi, K. Fueki, Yogyo-Kyokai-Shi, 88 (1980) 741.

[20] R. Beerkens, P. Laimbök, S. Kobayashi, Ceram. Trans. 82 (1998) 43.

[21] J. J. Hammel, Advances in Ceramics, 18 (1986) 177.

[22] F. E. Woolley, Engineered Materials Handbook, 4 (1991) 386.

Figure captions

Fig. 1. Experimental set-up for the study of E-glass foaming under controlled atmospheres

Fig. 2. Sample height versus time in the E-glass batch ramp-heated at 10°C/min (lines connect the data points measured at 1 min interval – same for Figs. 3 through 8)

Fig. 3. Sample height versus time in the E-glass batch ramp-heated at 5°C/min

Fig. 4. Sample height per unit mass of batch versus temperature

Fig. 5. ψ and furnace temperature versus time (t = 0 at T = 1300°C) for the tests with air flow

Fig. 6. ψ and furnace temperature versus time for tests in air-based atmospheres

Fig. 7. ψ and furnace temperature versus time for tests in CO_2-based atmospheres

Fig. 8. ψ and furnace temperature versus time for tests in dry atmospheres

Fig. 9. Maximum ψ versus H_2O content (lines were drawn as guides to the eyes – same for Figs. 10 through 13)

Fig. 10. ψ increase rate ($d\psi/dT$) versus H_2O content

Fig. 11. Foam collapse time to 50% of maximum ψ versus H_2O content

Fig. 12. Foam collapse time to 25% of maximum ψ versus H_2O content

Fig. 13. SO_3 wt% measured in glasses after heating to 1250 or 1500°C under various atmospheres

Table 1

Test Conditions and Target Gas Compositions

Test #	Atmosphere introduced from 1250°C	Gas Volume %			
		N_2	O_2	CO_2	H_2O
1	Air	80	20		
2	Air, repeat of test #1	80	20		
3	Air, higher flow rate[(a)]	80	20		
4	Air + 20% H_2O	64	16		20
5	Air + 55% H_2O	36	9		55
6	CO_2			100	
7	CO_2 + 20% H_2O			80	20
8	CO_2 + 55% H_2O			45	55
9	90% (CO_2 + 55% H_2O) + 10% O_2		10	40.5	49.5
10	CO_2 + 20% O_2		20	80	
11	CO_2 + 20% N_2	20		80	
12	CO_2 + 80% N_2	80		20	
13	CO_2 + 55% H_2O[(b)]			45	55

(a) The flow rate of 90 cm^3/min instead of 40 cm^3/min used for all other tests.
(b) Gas was introduced from 300°C instead of 1250°C.

Table 2

Maximum ψ, ψ increase rates, foaming temperature, and foam collapse times for all foaming tests

Test #	Atmosphere introduced from 1250°C	Max ψ	ψ increase rate		Time range for r_ψ (min)	Foam starting Temp. (°C)	Foam collapse time (min)[(a)]	
			$r_\psi = d\psi/dt$	$d\psi/dT$			$t_{0.5}$	$t_{0.25}$
1	Air	6.52	0.27	0.058	15 - 25	1365	16	-
2	Air, repeat of #1	7.03	0.33	0.070	17 - 26	1368	22	-
3	Air, higher flow rate, 90 cm^3/min	7.44	0.40	0.089	21 - 28	1385	14	-
4	Air + 20% H_2O	7.59	0.40	0.090	21 - 28	1375	15	31
5	Air + 55% H_2O	5.93	0.37	0.079	24 - 32	1404	10	13
6	CO_2	8.55	0.44	0.108	21 - 29	1385	14	28
7	CO_2 + 20% H_2O	7.86	0.45	0.095	18 - 25	1374	11	15
8	CO_2 + 55% H_2O	6.08	0.40	0.086	18 - 24	1377	12	14
9	90% (CO_2 + 55% H_2O) + 10% O_2	6.04	0.42	0.088	17 - 25	1373	12	19
10	CO_2 + 20% O_2	8.09	0.41	0.090	18 - 29	1377	10	10
11	CO_2 + 20% N_2	8.41	0.42	0.087	24 - 30	1378	15	-
12	CO_2 + 80% N_2	8.13	0.42	0.090	20 - 28	1383	14	25
13	CO_2 + 55% H_2O, introduced at 300°C	Did not foam						

(a) Time to reach the specified fraction of the maximum ψ.

Table 3

SO_3 wt% measured in glasses after heating to 1250 or 1500°C under various atmospheres

Test #	300 - 1250°C	1250 - 1500°C	SO_3 wt%
1	Ambient	Air flow	0.083
8	Ambient	CO_2 + 55% H_2O	0.050
13	CO_2 + 55% H_2O	CO_2 + 55% H_2O	0.032
1a (or 8a)	Ambient	N/A	0.187
13a	CO_2 + 55% H_2O	N/A	0.035

N/A: not applicable; heating was stopped at 1250°C.

Fig. 1

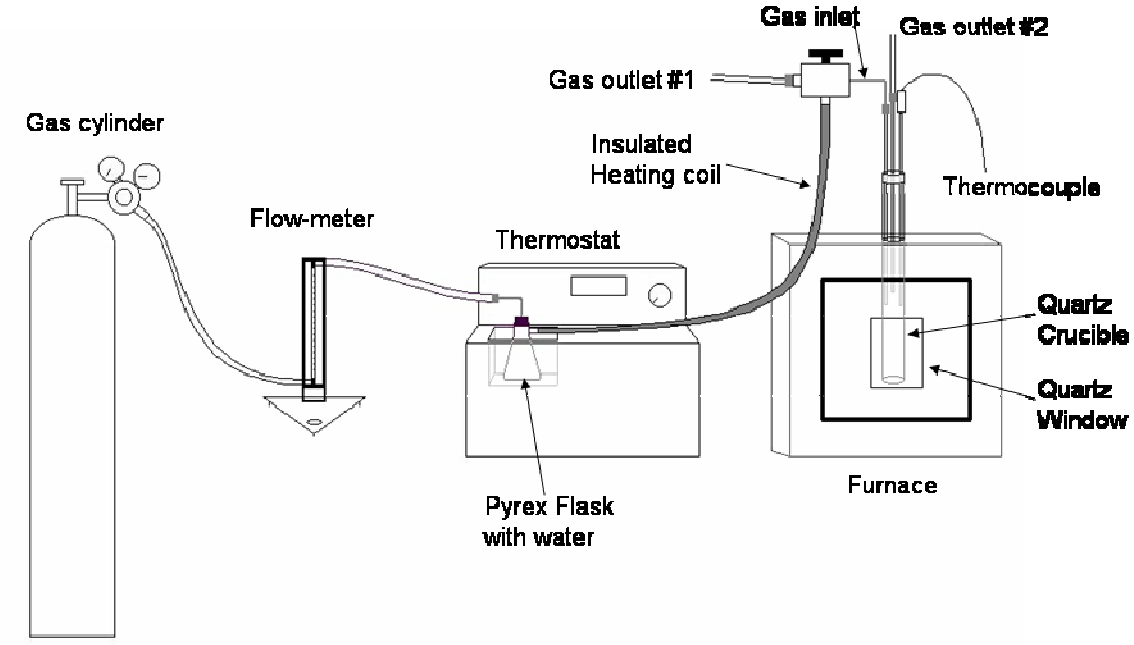
Gas inlet
Gas outlet #2
Gas outlet #1
Gas cylinder
Insulated
Heating coil
Thermocouple
Flow-meter
Thermostat
Quartz
Crucible
Quartz
Window
Furnace
Pyrex Flask
with water

Fig. 2

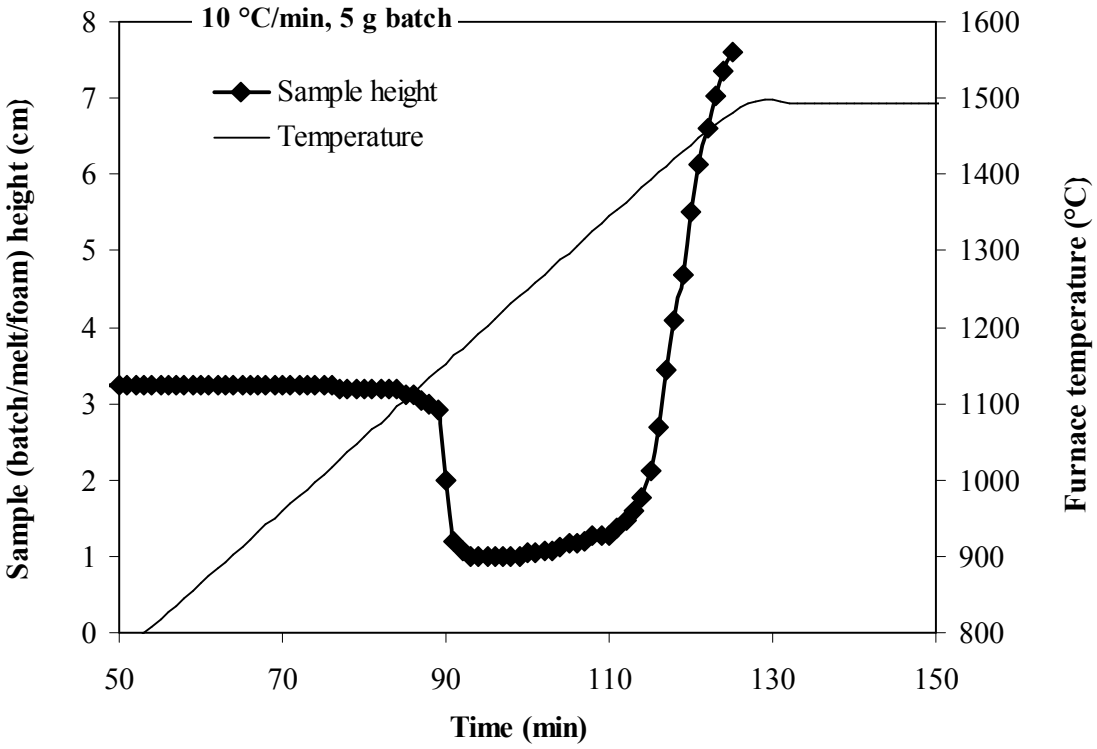
10 °C/min, 5 g batch
Sample height
Temperature
Sample (batch/melt/foam) height (cm)
Furnace temperature (°C)
Time (min)
0
1
2
3
4
5
6
7
8
800
900
1000
1100
1200
1300
1400
1500
1600
50
70
90
110
130
150

Fig. 3

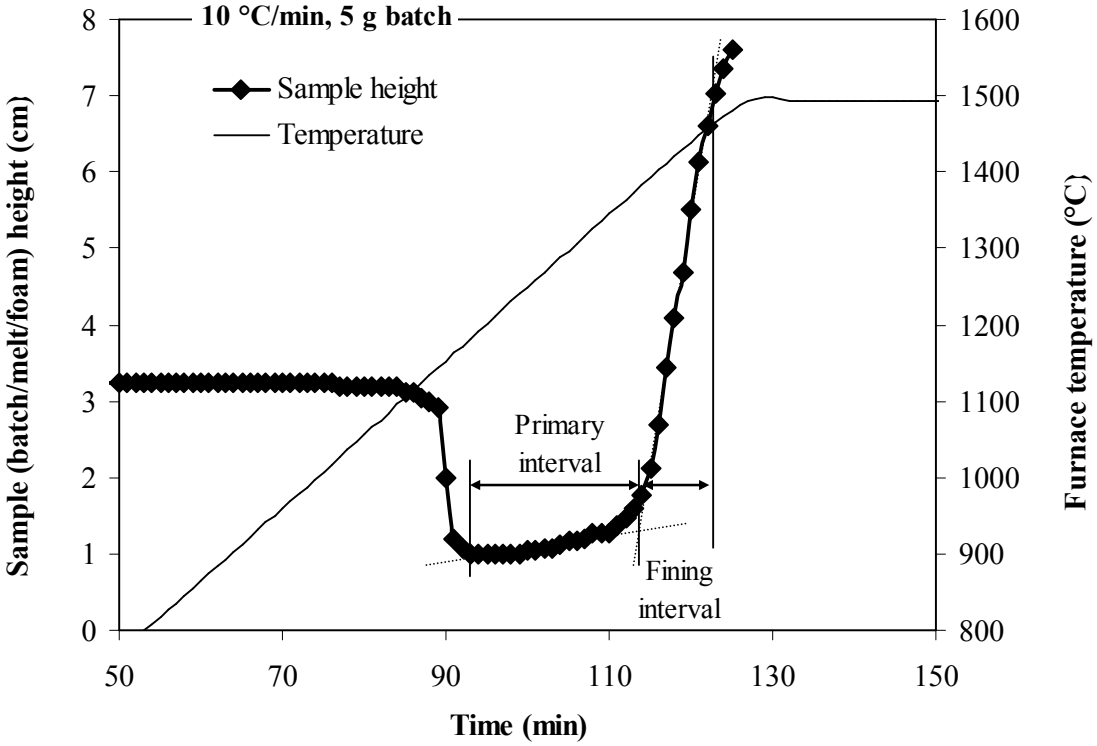
10 °C/min, 5 g batch
Sample height
Temperature
Primary interval
Fining interval
Sample (batch/melt/foam) height (cm)
Furnace temperature (°C)
Time (min)
0
1
2
3
4
5
6
7
8
800
900
1000
1100
1200
1300
1400
1500
1600
50
70
90
110
130
150

Fig. 4

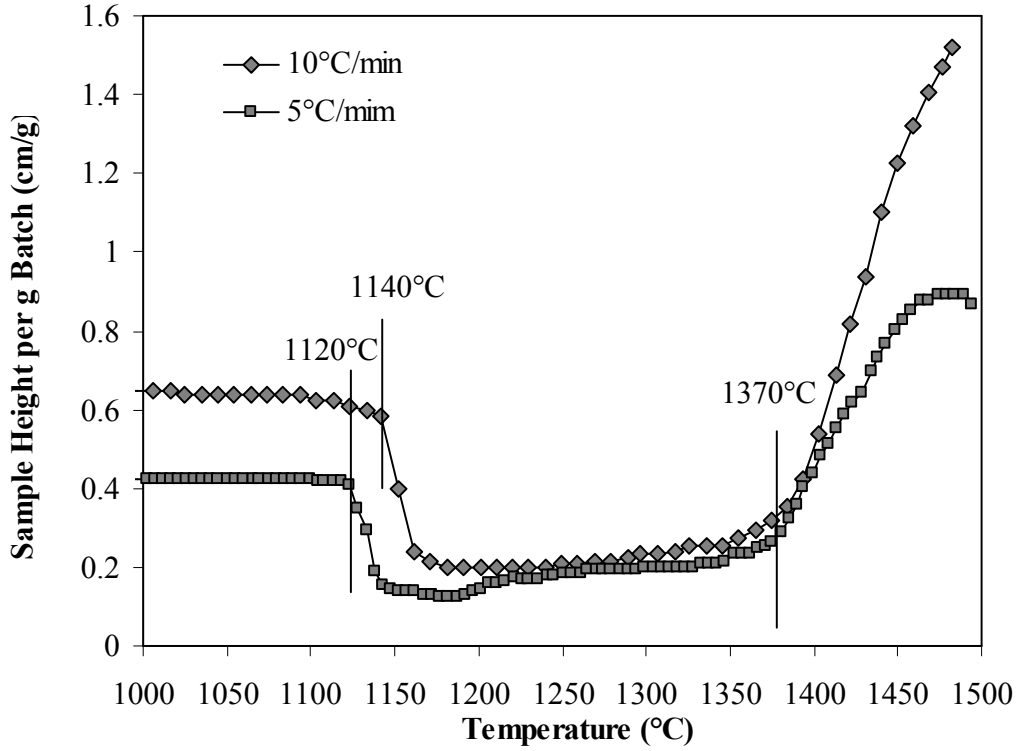
10°C/min
5°C/mim
1140°C
1120°C
1370°C
Sample Height per g Batch (cm/g)
Temperature (°C)
1.6
1.4
1.2
1
0.8
0.6
0.4
0.2
0
1000 1050 1100 1150 1200 1250 1300 1350 1400 1450 1500

Fig. 5

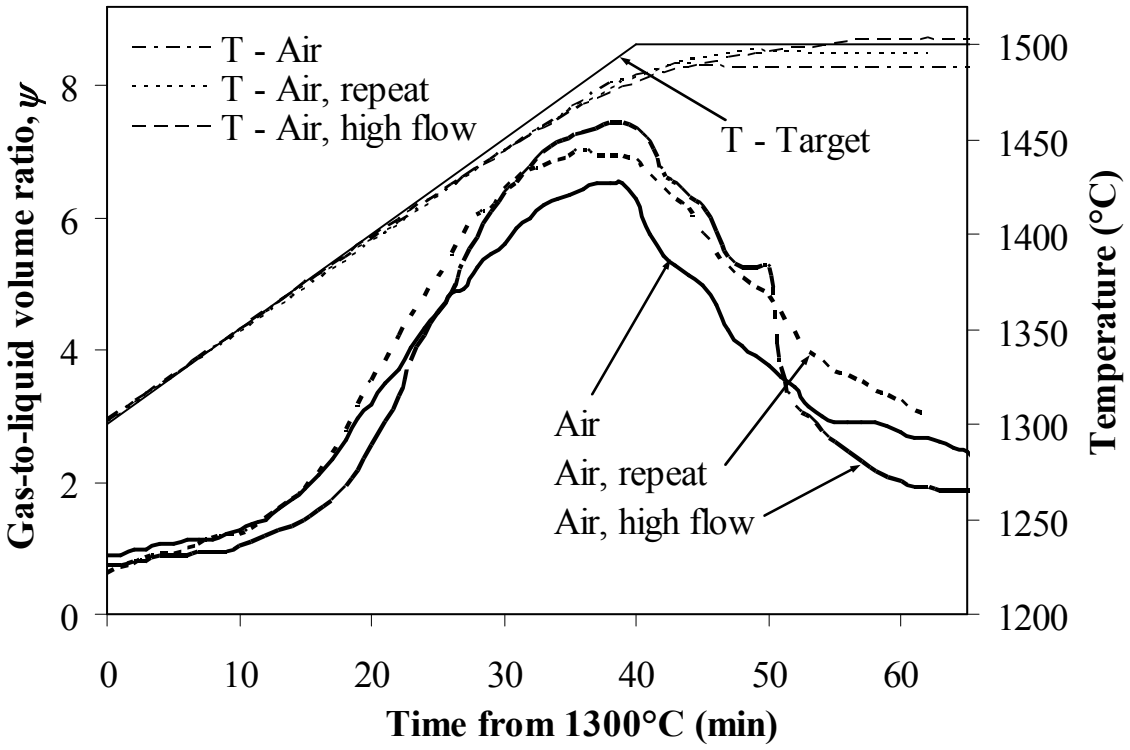
T - Air
T - Air, repeat
T - Air, high flow
T - Target
Air
Air, repeat
Air, high flow
Gas-to-liquid volume ratio, ψ
Temperature (°C)
Time from 1300°C (min)
0
2
4
6
8
1200
1250
1300
1350
1400
1450
1500
0
10
20
30
40
50
60

Fig. 6

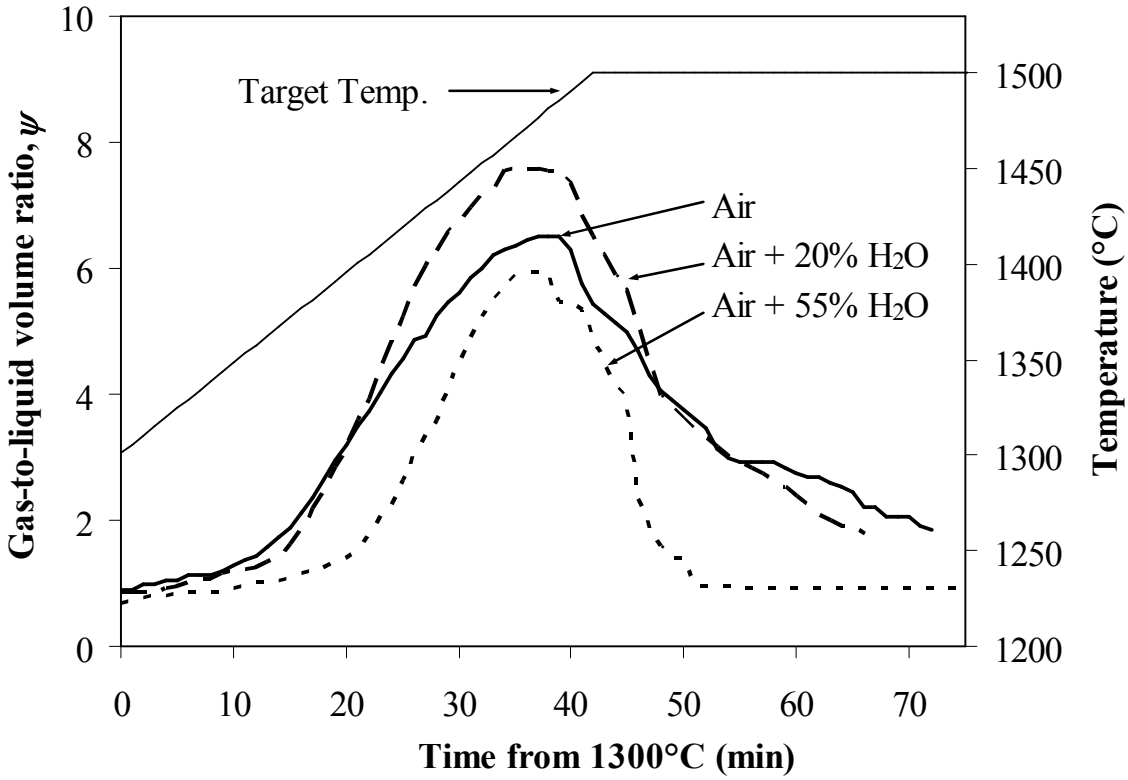
Target Temp.
Air
Air + 20% H2O
Air + 55% H2O
Gas-to-liquid volume ratio, ψ
Temperature (°C)
Time from 1300°C (min)
0
2
4
6
8
10
1200
1250
1300
1350
1400
1450
1500
0
10
20
30
40
50
60
70

Fig. 7

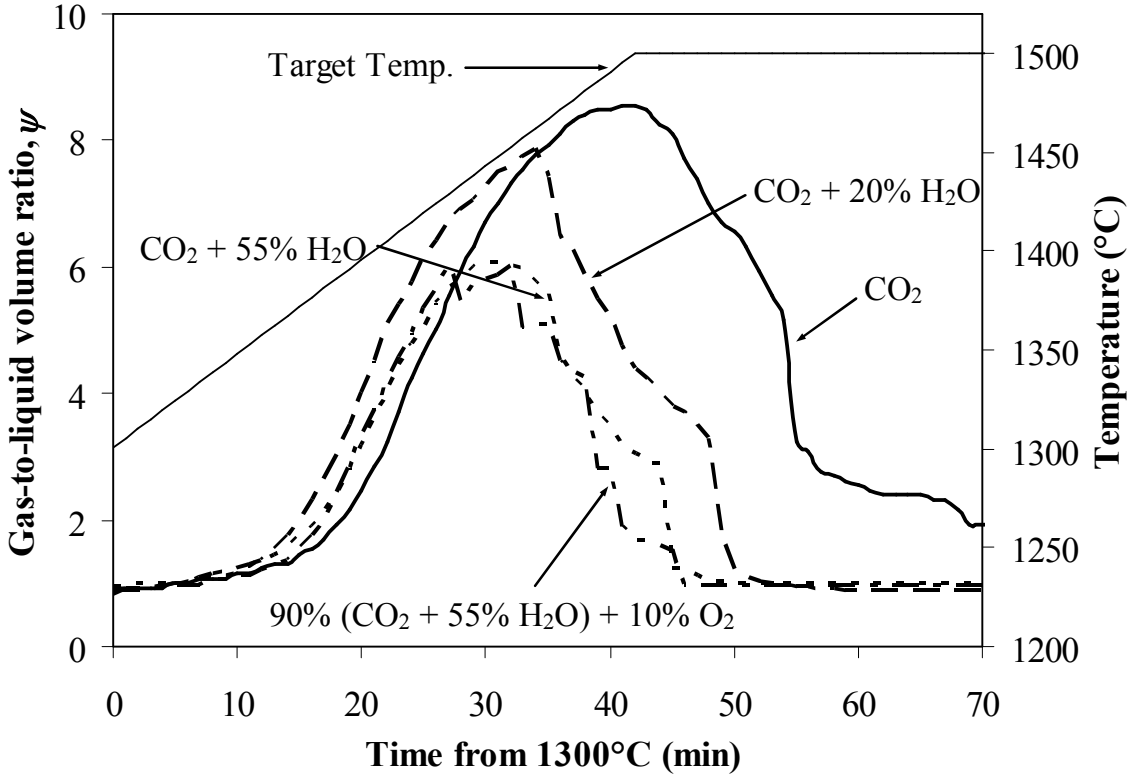
Target Temp.
CO2 + 20% H2O
CO2 + 55% H2O
CO2
90% (CO2 + 55% H2O) + 10% O2
Gas-to-liquid volume ratio, ψ
Temperature (°C)
Time from 1300°C (min)
0
2
4
6
8
10
1200
1250
1300
1350
1400
1450
1500
0
10
20
30
40
50
60
70

Fig. 8

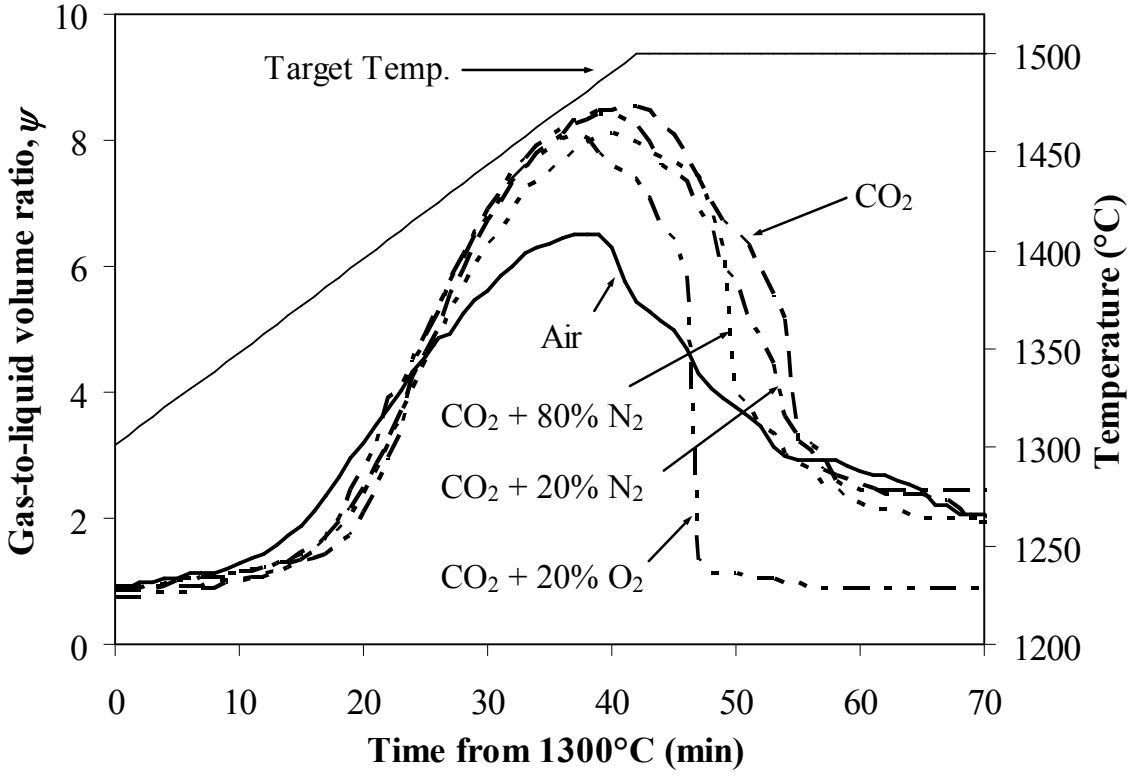
Target Temp.
CO2
Air
CO2 + 80% N2
CO2 + 20% N2
CO2 + 20% O2
Gas-to-liquid volume ratio, ψ
Temperature (°C)
Time from 1300°C (min)
0
2
4
6
8
10
1200
1250
1300
1350
1400
1450
1500
0
10
20
30
40
50
60
70

Fig. 9

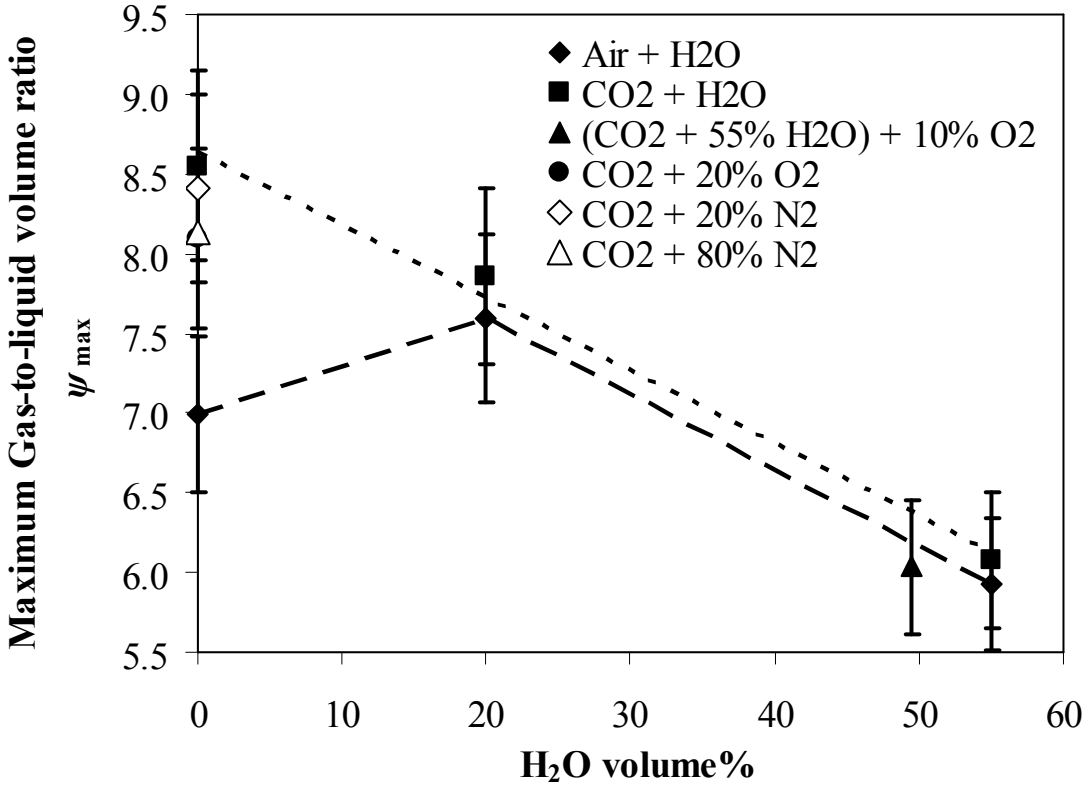
Maximum Gas-to-liquid volume ratio
ψ_{max}
9.5
9.0
8.5
8.0
7.5
7.0
6.5
6.0
5.5
0
10
20
30
40
50
60
H_2O volume%
Air + H2O
CO2 + H2O
(CO2 + 55% H2O) + 10% O2
CO2 + 20% O2
CO2 + 20% N2
CO2 + 80% N2

Fig. 10

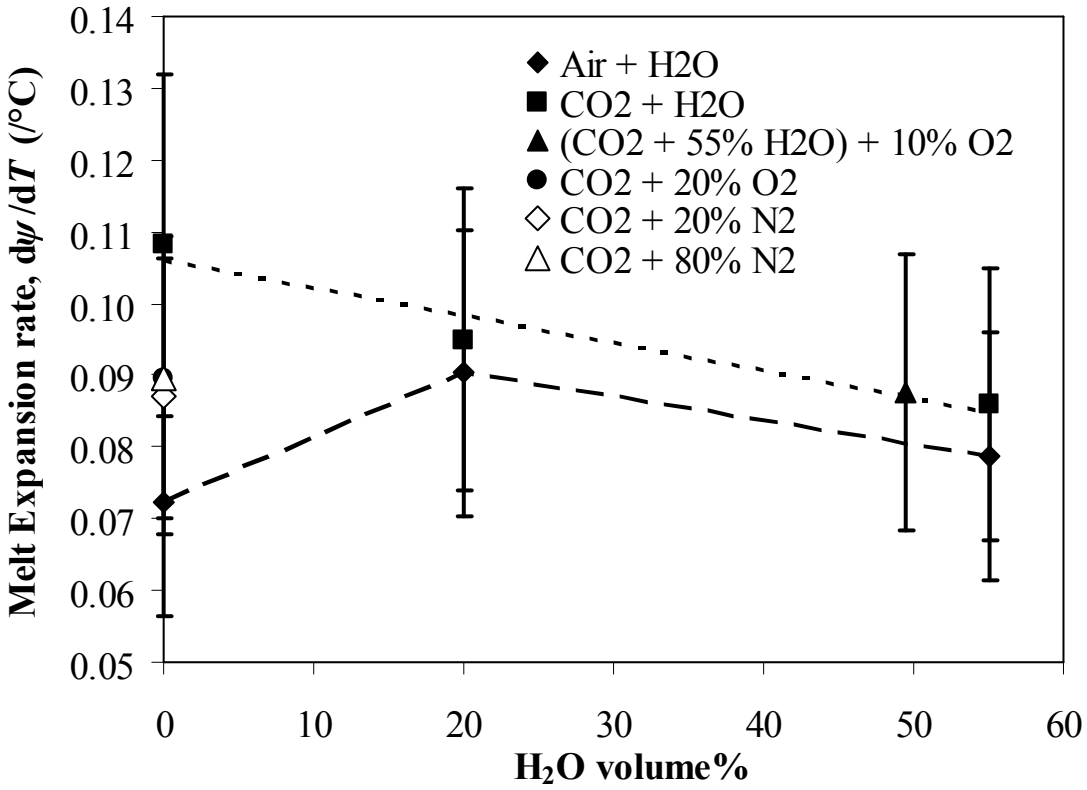
0.14
0.13
0.12
0.11
0.10
0.09
0.08
0.07
0.06
0.05
Melt Expansion rate, dψ/dT (/°C)
Air + H2O
CO2 + H2O
(CO2 + 55% H2O) + 10% O2
CO2 + 20% O2
CO2 + 20% N2
CO2 + 80% N2
0
10
20
30
40
50
60
H2O volume%

Fig. 11

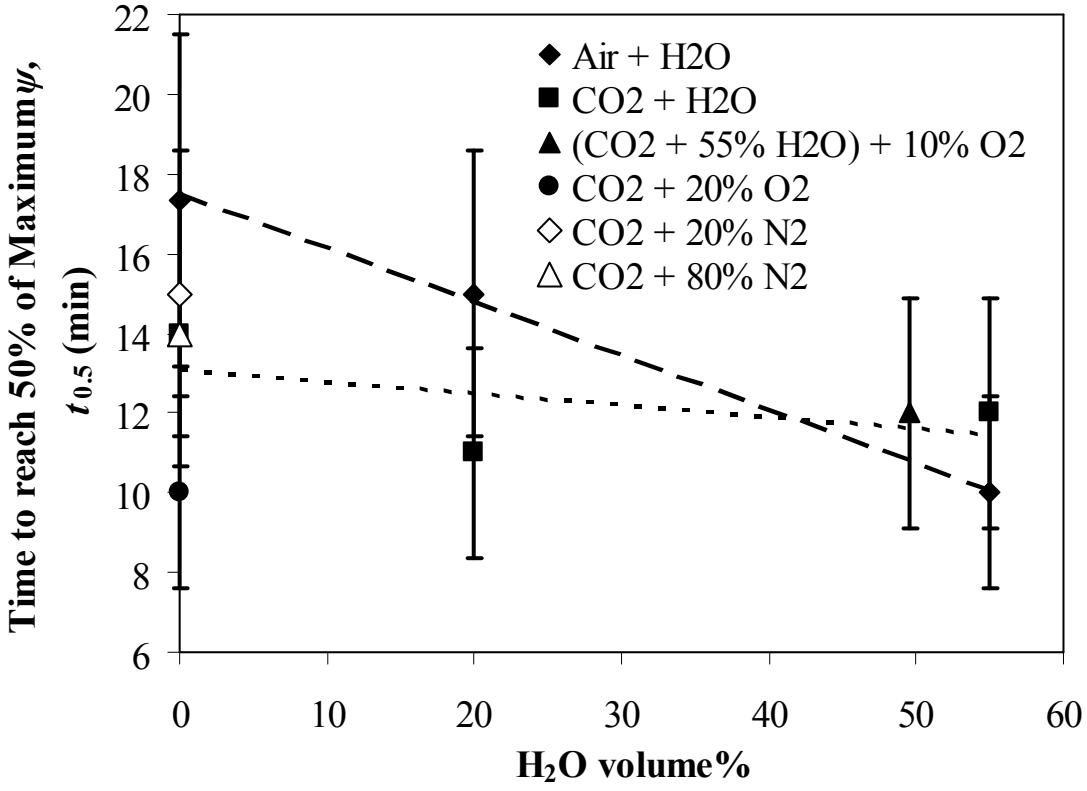
Time to reach 50% of Maximum ψ, $t_{0.5}$ (min)
22
20
18
16
14
12
10
8
6
0
10
20
30
40
50
60
H_2O volume%
Air + H2O
CO2 + H2O
(CO2 + 55% H2O) + 10% O2
CO2 + 20% O2
CO2 + 20% N2
CO2 + 80% N2

Fig. 12

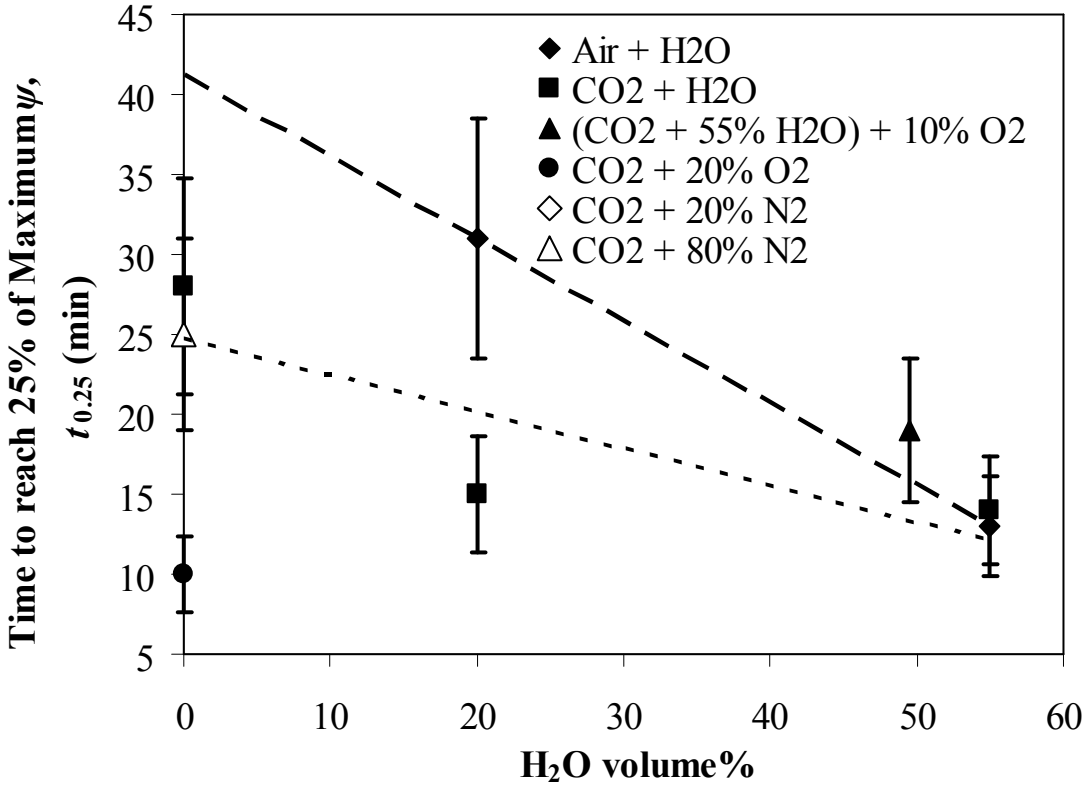
Time to reach 25% of Maximum ψ, $t_{0.25}$ (min)
45
40
35
30
25
20
15
10
5
0
10
20
30
40
50
60
H2O volume%
Air + H2O
CO2 + H2O
(CO2 + 55% H2O) + 10% O2
CO2 + 20% O2
CO2 + 20% N2
CO2 + 80% N2

Fig. 13

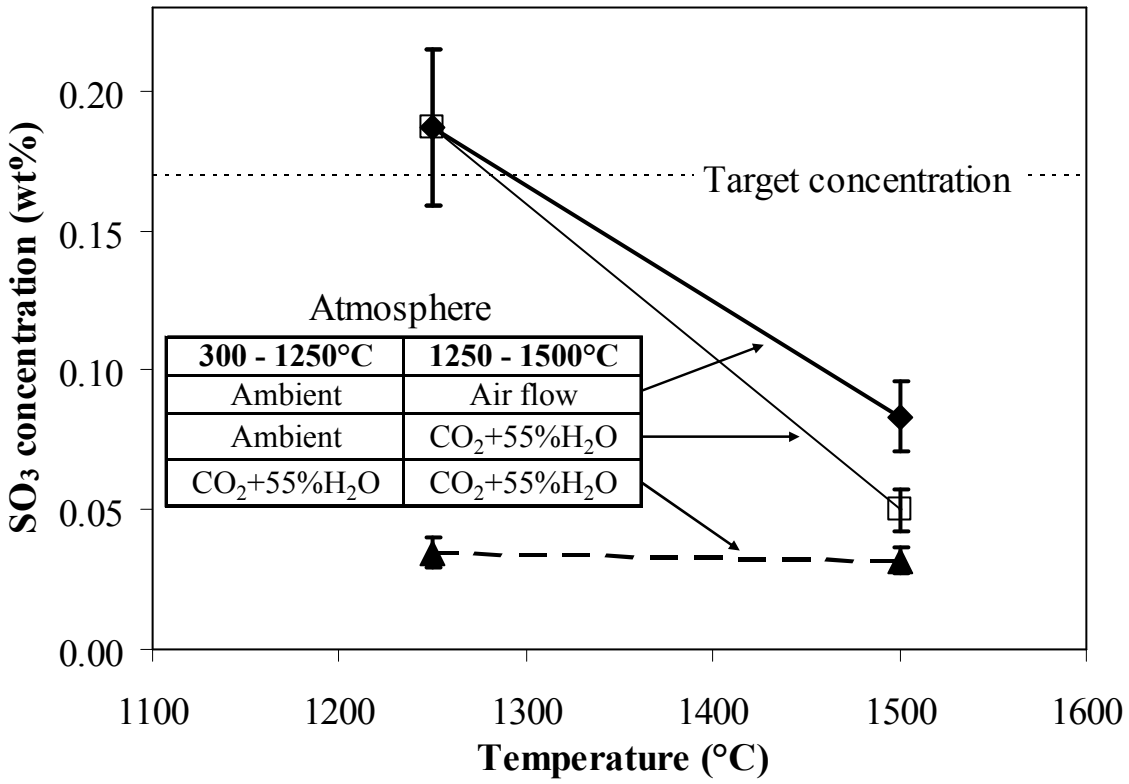
0.20
0.15
0.10
0.05
0.00
SO3 concentration (wt%)
Target concentration
Atmosphere
300 - 1250°C
1250 - 1500°C
Ambient
Air flow
Ambient
CO2+55%H2O
CO2+55%H2O
CO2+55%H2O
1100
1200
1300
1400
1500
1600
Temperature (°C)